Nano Energy 40 (2017) 655–662

Contents lists available at ScienceDirect

Nano Energy

journal homepage: www.elsevier.com/locate/nanoen

Communication

Freestanding carbon encapsulated mesoporous vanadium nitride nanowires enable highly stable sulfur cathodes for lithium-sulfur batteries

Xingxing Li[a], Kang Ding[a], Biao Gao[a,*], Qingwei Li[b], Yuanyuan Li[b], Jijiang Fu[a], Xuming Zhang[a], Paul K. Chu[c], Kaifu Huo[b,*]

[a] The State Key Laboratory of Refractories and Metallurgy, School of Materials and Metallurgy, Wuhan University of Science and Technology, Wuhan 430081, China
[b] Wuhan National Laboratory for Optoelectronics (WNLO) and School of Optical and Electronic Information, Huazhong University of Science and Technology, Wuhan 430074, China
[c] Department of Materials Science and Physics, City University of Hong Kong, Tat Chee Avenue, Kowloon, Hong Kong, China

ARTICLE INFO

Keywords:
Vanadium nitride
Chemical anchoring
Physical trapping
Polysulfides
Sulfur cathodes
Lithium-sulfur battery

ABSTRACT

Lithium-sulfur (Li-S) battery is one of the most promising energy storage systems due to its large energy density of 2560 Wh kg^{-1}. However, severe shuttle effect of polysulfide intermediates, poor conductivity of S and large volume change during cycling cause fast capacity fading and poor cycle performance. Herein, we demonstrate S nanodots impregnated microporous carbon encapsulated conductive mesoporous vanadium nitride nanowires (S/MVN@C NWs) as high-performance S cathode materials for Li-S batteries. The S nanodots with the size of 2–5 nm are impregnated into the mesopores of MVN@C NWs and further encapsulated with microporous carbon. During cycling, the polysulfides intermediates are strongly chemical anchored by the conductive MVN NWs and further physically trapped by microporous carbon coating within the cathode. The freestanding and binder-free cathode comprising intertwining and interpenetrating S/MVN@C NWs demonstrates highly mechanical flexibility, which deliver a long cycle life of 636 mAh g^{-1} after 200 cycles at 1 C (1650 mA g^{-1}) and high rate performance with a capacity of 543 mAh g^{-1} at 10 C. Even at a high areal mass loading of 9.7 mg cm^{-2}, a large and stable capacity of 7.1 mAh cm^{-2} is achieved. The strategy combining microporous carbon coating with high conducting mesoporous metal nitrides opens a feasible route to design large-capacity and high-stability S-based cathodes for Li-S batteries.

1. Introduction

The large demand for portable electronics, electronic vehicles, and intermittent renewable energy sources has spurred the development of advanced energy storage systems and devices [1,2]. Lithium-sulfur (Li-S) batteries are regarded as one of the most promising energy storage systems due to the large theoretical energy density of 2560 Wh kg^{-1}, which is much larger than that of commercial lithium-ion batteries composed of graphite anode and $LiCoO_2$ cathode. Moreover, sulfur (S) is abundant, low-cost, and environmentally friendly. However, development of Li-S batteries has been hampered by the poor cycling stability, limited S electrochemical utilization and low rate capability mainly due to the poor conductivity of S and its discharge products, severe shuttle effect of soluble lithium polysulfides (Li_2S_n, n = 3–8), and 80% volume expansion of S after full lithiation [3–5]. Many strategies have been explored to design and engineer S-based cathodes to ameliorate the Li storage properties, mainly by improving the conductivity of the electrodes and reducing the shuttle effect of polysulfides. Carbon (C) materials such as carbon nanotubes, graphene, activated C, and carbon hollow spheres are widely used as S hosts in Li-S batteries due to the large surface area and high conductivity [6–9]. Compared to pure S, S/C composites show improved cycling life by physically confining the Li_2S_n in the pores or carbon host layers [10,11]. However, the weak interaction between non-polar hydrophobic carbon and polar hydrophilic Li_2S_n species undermines the application of carbon in Li-S batteries as polysulfide traps. Recently, polar metal oxides such as SiO_2 [12], TiO_2 [13], Al_2O_3 [14,15], MnO_2 [16], Ti_4O_7 [17] and V_2O_5 [18] as well as metal sulfides including TiS_2 [19], WS_2 [20], and CoS_2 [21] have been proposed as effective polysulfide adsorbents or trappers by utilizing the strong chemical interaction to prolong the cycling life. Nevertheless, most metal oxides and sulfides are not conductive and impede electron transport, resulting in low S utilization and poor rate performance [22–24]. Compared to metal oxides, transitional metal nitrides (TMNs) possess higher electrical conductivity. Very recently, mesoporous TMNs such as VN, TiN, and Mo_2N have been proposed as superior capacitive materials for supercapacitors (SCs) [25–27]. Owing

* Corresponding authors.
E-mail addresses: gaobiao@wust.edu.cn (B. Gao), kfhuo@hust.edu.cn (K. Huo).

http://dx.doi.org/10.1016/j.nanoen.2017.09.018
Received 2 June 2017; Received in revised form 7 September 2017; Accepted 7 September 2017
Available online 09 September 2017

to the high conductivity, good structural stability and strong chemical anchoring effect towards Li_2S_n species, TMNs should be promising S host materials in highly stable Li-S batteries. Recently, Goodenough et al. reported mesoporous TiN-S cathode for stable Li-S batteries [28] and Li et al. developed a conductive porous VN nanoribbon/graphene composite for Li-S batteries [29]. Despite the great promise, the drawback of TMNs in advanced Li-S batteries is the small surface area, small pore volume, and open access structure. The large and open accessible mesopores of TMNs cannot efficiently suppress outward diffusion of Li_2S_n, especially with a large S concentration, thus leading to unsatisfactory capacity retention and cycle life. Hence, it is crucial to design and develop high-performance S host materials that not only offer strong anchoring to soluble Li_2S_n species, but also possess high intrinsic electronic conductivity for boasting good Li-S battery performance even at large current densities.

Among TMN candidates, VN is considered as most promising candidates for SCs because it possesses high electrical conductivity (σ_{bulk} = $1.67 \times 10^6\ \Omega^{-1}\,m^{-1}$), which are much higher than that of the V_2O_5 [25,29]. Here, conductive mesoporous VN nanowires encapsulated with conductive C (MVN@C NWs) are described as high-performance S host materials for advanced S cathodes of Li-S batteries. The S impregnated MVN@C NWs (S/MVN@C NWs) cathode has the following advantages: (1) the inner mesopores of the MVN core offer nano-scale containers for active S and S nanodots are mainly stitched into the mesopores of VN providing short electron/ion transfer paths; (2) the soluble Li_2S_n intermediates are chemically tethered by mesoporous VN [29] and further physically trapped by the microporous C shell [23], thereby effectively inhibiting outward diffusion and the shuttle effect of soluble Li_2S_n; (3) the mesopores space of the inner MVN buffers the stress originating from the volume changes of S during charging/discharging processes, resulting in high structure stability of the electrode; (4) VN possesses catalytic properties similar to precious metals thus facilitating the redox reaction kinetics [29]; (5) the conductive and long S/MVN@C NWs are interpenetrated and intertwined together to form a freestanding/binder-free three dimensional (3D) conductive network without a conductive additive or other mechanical supporter, and hence, the paper-like flexible film cathode has a large overall capacity and is suitable for flexible Li-S batteries. With a large S content of 57.2 wt% and areal mass loading of 2.8 mg cm^{-2}, the freestanding and binder-free S/MVN@C NWs cathode delivers a large initial capacity of 1305 mAh g^{-1} at 0.2 C (1 C = 1650 mA g^{-1}), a long cycle life over 200 cycles with a capacity of 636 mAh g^{-1} and a high rate capacity of 543 mAh g^{-1} at 10 C. Moreover, a large and stable areal capacity of 7.1 mAh cm^{-2} is achieved at a high mass loading of 9.7 mg cm^{-2}, offering promising applications in high-energy Li-S batteries.

2. Experimental section

2.1. Preparation of S/MVN@C NWs

2.1.1. Synthesis of V_2O_5 NWs

Firstly, 0.364 g of V_2O_5 powders (99%, Sigma-Aldrich) were mixed with 30 mL of deionized water (DW), followed by adding of 5 mL of H_2O_2 (30%, Sigma-Aldrich) under vigorous stirring. Then, the mixture solution was transferred into a 60 mL Teflon-lined autoclave and kept at 210 °C for 72 h. The yellow product of V_2O_5 nanowires was produced via washing with ethanol and DW for several times.

2.1.2. Synthesis of MVN@C NWs

The as-prepared V_2O_5 NWs were dispersed in Tris-HCl buffer (99%, Sigma-Aldrich) solution with the concentration of 10 mM and the pH value of 8.5, then dopamine (DA, Sigma-Aldrich) with the concentration of 1 mg mL^{-1} were added into above solution. After magnetic stirring and polymerization for 30 min, the dark polydopamine coated V_2O_5 nanowires (V_2O_5@PDA NWs) film were produced by vacuum filtering after washing with DW for three times. The resultant freestanding film of MVN@C NWs were obtained by further annealing freestanding V_2O_5@PDA NWs film at 750 °C for 3 h under the NH_3 atmosphere. The thickness of MVN@C NWs film can be easily adjusted by changing the mass of MVN@C NWs. For comparison, we synthesized the mesoporous MVN NWs by directly nitriding as-prepared V_2O_5 NWs. The N-doping carbon nanotubes (NCNT) were also fabricated by dissolving MVN@C NWs in 6 M KOH solution to remove the MVN core.

2.1.3. Synthesis of S/MVN@C NWs

A S/carbon disulfide (CS_2) solution was firstly prepared by dissolving S into CS_2 with the concentration of 0.15 g mL^{-1}, and then paper-like MVN@C film (8 × 25 mm^2) was soaked into S/CS_2 mixed solution for 30 min. Subsequently, the film was taken out, put into the glass tube, which was heated at 155 °C for 12 h to ensure that the S is fully impregnated into the MVN@C NWs. The S impregnated MVN@C NWs samples with different S mass loading could be obtained by changing the content of sulfur in S/CS_2 mixed solution. The S impregnated MVN NWs (S/MVN NWs) and the S impregnated NCNT (S/NCNT) were produced in the similar way.

2.2. Polysulfide adsorption test

A polysulfide catholyte was prepared by chemically reacting of sublimed sulfur and lithium sulfide at a molar ratio of 5:1 in an appropriate amount of 1,2-dimethoxyethane (DME) and 1,3-dioxolane (DOL) (1:1, ratio by volume) by vigorous magnetic stirring at 50 °C. Then, equivalent amounts (25 mg) of MVN@C NWs, MVN NWs, and NCNT were immersed into 3 mL of polysulfide catholyte with a concentration of 5 mM for Li_2S_6, respectively. After stewing for 24 h, digital photos were taken to show the color change of above samples.

2.3. Materials characterization

The morphology and structure of the as-obtained samples were characterized using field-emission scanning electron microscopy (SEM, FEI Nova 450 Nano) and high-resolution transmission electron microscopy (TEM, FEI Titan G2 60-300) equipped with energy-dispersive X-ray spectroscopy (EDX, Oxford). X-ray diffraction (XRD, Philips X′ Pert Pro (Cu Kα radiation, λ = 1.5418 Å)), Raman scattering (HR RamLab) and X-ray photoelectron spectroscopy (XPS, ESCALB MK-II) were employed to analyze the structure and component of above samples. The concentration of polysulfide catholyte was evaluated by ultraviolet-visible (UV–Vis, Shimazu UV-2550). The N_2 adsorption-desorption curves were evaluated using Micromeritics ASAP 2020 analyzer. The average pore distribution were calculated using Barrett-Joyner-Halenda and Density Functional Theory models for mesopores and micropores, respectively. The thermal analysis was performed with Naichi Corporation STA449 in Ar atmosphere at 10 °C min^{-1} from room temperature to 600 °C. We also measured the conductivity of the film electrodes by four-tip probes method. The conductivity of the VN and MVN@C NWs film electrodes are about 4.3×10^4 and $3.46 \times 10^4\ \Omega^{-1}\,m^{-1}$. After S impregnation with 57.2% mass loading, S/MVN@C NWs films still exhibits a high conductivity of $2.3 \times 10^4\ \Omega^{-1}\,m^{-1}$.

2.4. Electrochemical measures

The paper-like binder-free film of the S/MVN@C NWs, S/MVN NWs and S/NCNT were cut into square plate (4 × 4 mm^2). The coin-like 2016 type cells were assembled with the above electrodes as the cathode and lithium foil as anode. DOL/DME (1:1, v/v) with 1 M lithium bis (trifluoromethanesulfonyl) and 0.1 M $LiNO_3$ was used as the electrolyte and Celgard 2300 film as separator. Cyclic voltammogram (CV) profiles were acquired from electrochemical work station (CHI 760e) at the scan rate of 0.1 mV s^{-1}. Galvanostatic discharge-charge tests at different current densities (based on the mass of sulfur) were

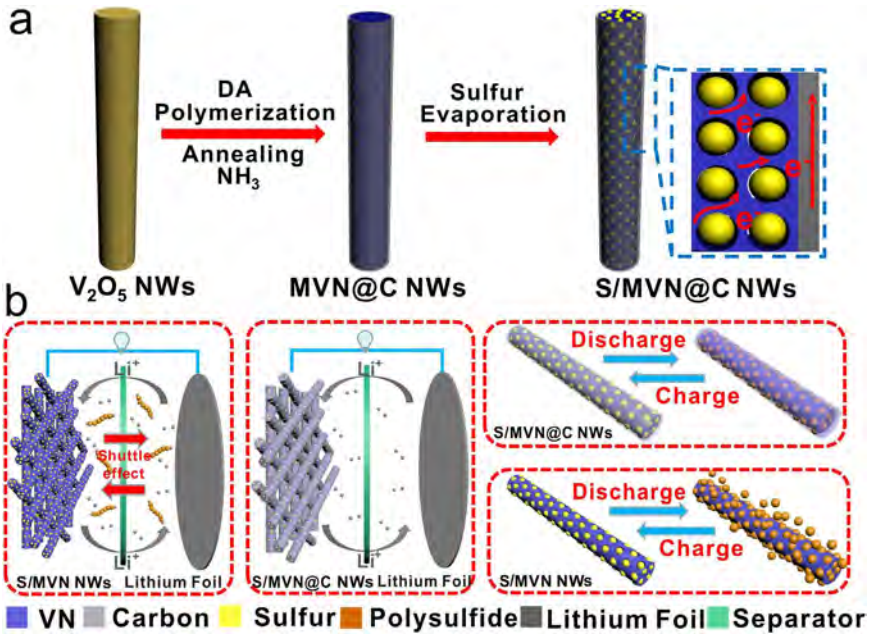

Fig. 1. (a) Schematic diagram illustrating the procedures to prepare S/MVN@C NWs. (b) Illustration of S/MVN@C NWs and S/MVN NWs cathodes during cycling.

performed on electrochemical test system (Land CT2001A) in the voltage window from 1.6 to 3.0 V.

3. Results and discussion

The fabrication process of the S/MVN@C NWs is schematically shown in Fig. 1a. The V_2O_5 NWs with an average diameter of 100 nm and tens of micrometers long (Figs. S1a-b, Supporting information) are synthesized hydrothermally with V_2O_5 powder and H_2O_2 as precursors. The resultant V_2O_5 NWs with large aspect ratio not only have wide applications for energy conversion and storage but also are promising self-templates for fabricating high conducting VN NWs by simple nitridation [30–33]. The as-synthesized V_2O_5 NWs are coated with a layer of PDA by dopamine self-polymerization and then annealed in NH_3 atmosphere to produce the core-shell MVN@C NWs [33]. The scanning electron microscopy (SEM) images in Figs. S1c-d (Supporting information) exhibit that the overall morphology does not change after thermal nitridation, but the enlarged SEM image reveals the mesoporous structure of the inner NWs. The X-ray diffraction (XRD) pattern in Fig. S2a (Supporting information) can be assigned to cubic VN [25] and the Raman scattering spectrum shows the typical D-band and G-band of C (Fig. S2b, Supporting information), indicating the NWs are composed of VN and C. The transmission electron microscopy (TEM) image (Fig. S2c, Supporting information) confirms the core-shell structure with a C coating 10 nm in thickness and the VN NWs has a large number of mesopores $5-15$ nm in diameter. The mesoporous VN NWs provide a large amount of nano-reservoirs, which are beneficial for both S nanodots loading.

S is infiltrated into the MVN@C NWs by a melt-diffusion process at 155 °C to form S/MVN@C NWs. The SEM images in Fig. S3a-b (Supporting information) reveal that the overall morphology remains the same after S impregnation. However, the mesopores of the inner VN NWs couldn't be clearly identified from the enlarged SEM image, suggesting that the S nanodots fill into the mesopores of VN NWs. For comparison, MVN NWs without C coating (Figs. S3c-d, Supporting information) are prepared by nitriding as-synthesized V_2O_5 NWs and S is loaded into the MVN NWs using the similar method as S/MVN@C NWs. SEM and TEM images reveal that coarse S nanoparticles 20–40 nm in size after impregnation and the surface of MVN NWs is coated with of S (Figs. S3e-f, Supporting information). In contrast, S nanoparticles are not observed from the outside surface of the S/MVN@C NWs, suggesting that the presence of C shell effectively avoids the accumulation of S nanoparticles and carbon shell act as the "filtering layer" for S impregnation into MVN@C NWs. The Brunauer-Emmett-Teller (BET) surface area, pore size, and pore volume of MVN@C NWs is measured by nitrogen adsorption/desorption, which are shown in Fig. S4a (Supporting information). The pore size distribution curve of MVN@C NWs shows two peak at 0.4–0.7 nm and 4–15 nm. The mesopores in MVN@C NWs arise from the inner VN and micropores from the C coating as a result of pyrolysis of PDA under NH_3 atmosphere [33,34]. The measured surface area and pore volume are about 38.9 $m^2\ g^{-1}$ and of 0.084 $cm^3\ g^{-1}$, respectively. After S incorporation, the surface area and pore volume of the MVN@C NWs decrease to 23.7 $m^2\ g^{-1}$ and 0.053 $cm^3\ g^{-1}$ and the pore width of the mesopores also decreases (Fig. S4, Supporting information), further corroborating that S is impregnated into the MVN@C NWs. Assuming the 80% volume expansion of S forming Li_2S, the volume expansion of the impregnated S in full lithiation state is calculated to be 0.056 $cm^3\ g^{-1}$, which is smaller than the pore volume of MVN@C NWs (0.084 cm g^{-1}). Therefore, the MVN@C NWs could sufficiently accommodate the volume change of the impregnated S, resulting in high structure stability. TEM image of S/MVN@C NWs in full lithiation state remains intact, further confirming the high structure stability of S/MVN@C NWs during cycling (Fig. S5, Supporting information).

Although conductive VN has strong chemical interaction with polysulfides in the electrochemical process, MVN NWs could not fully inhibit the outward diffusion of polysulfides during cycling owing to large S particles coated on VN, as schematically shown in Fig. 1b. The size of Li_2S_n ($n = 5–8$) molecule is calculated to be about 0.5–0.7 nm at least two dimensions and micropores below/near this size can physically trap Li_2S_n [5]. The MVN@C NWs which combine the advantages of the microporous carbon coating and conductive mesoporous VN could effectively restrain the shuttle of soluble polysulfides by strong chemical anchoring of MVN and physical trapping of microporous C shell with the pore sizes are about 0.4–0.7 nm (Fig. S4, Supporting information), boasting better Li storage performance compared to MVN without C coating, as schematically described in Figs. 1a and b.

The typical high-resolution TEM image of S/MVN@C NWs is depicted in Figs. 2a and b, revealing that most of S nanodots with a size of 2–5 nm are filled into the mesopores of the MVN NWs (marked by white dotted line). Moreover, few S nanodots with the size of 1–2 nm embedded in the C coating are also observed (Fig. 2b) due to the presence

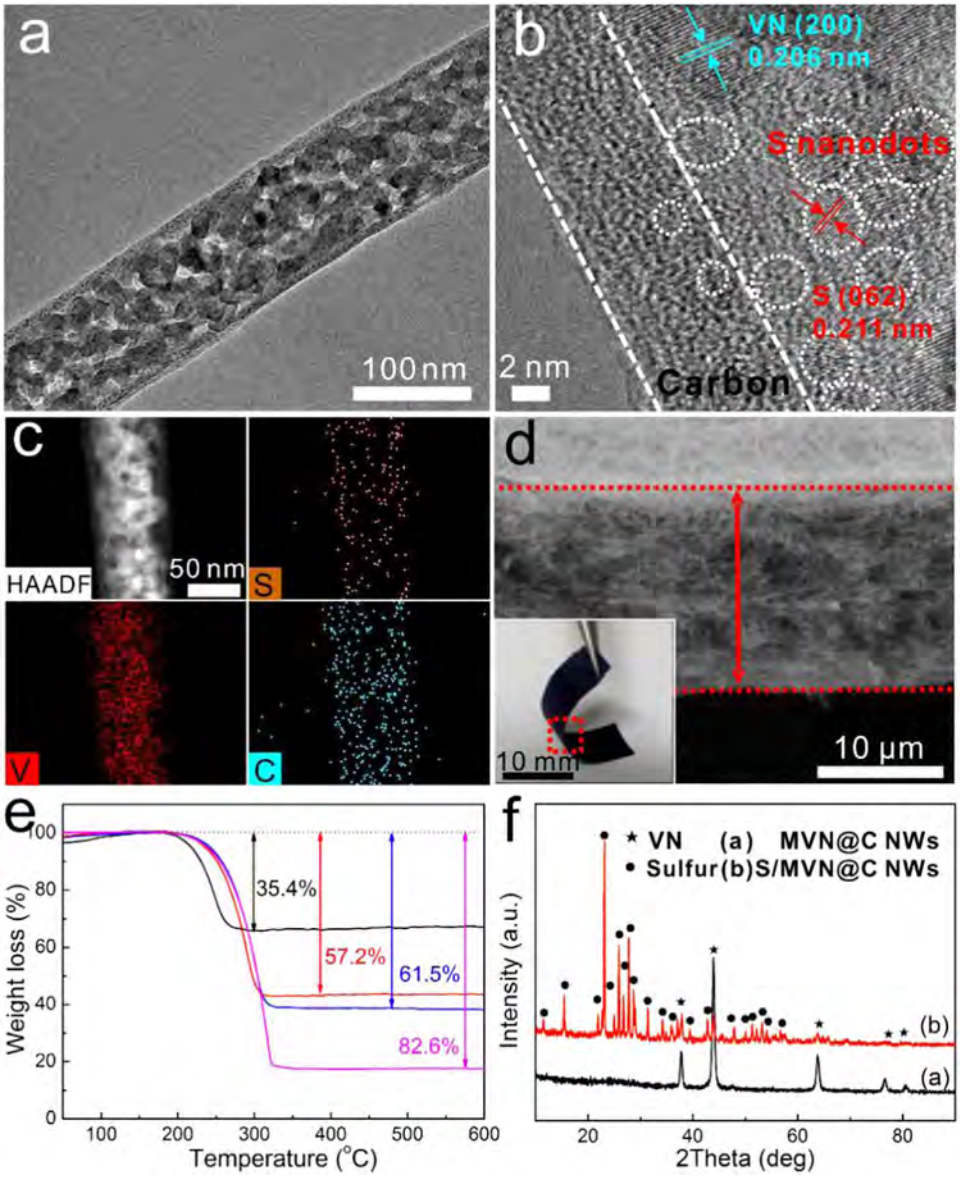

Fig. 2. (a) TEM image and (b) HR-TEM image of S/MVN@C NWs (S nanoparticles marked by white dotted line). (c) Scanning transmission electron microscopy (STEM) images of S/MVN@C NWs and corresponding elemental maps of S, V and C. (d) Cross-sectional SEM image of the self-supported S/MVN@C NWs film cathode with the inset showing the digital image of flexible film electrode. (e) TG curves of S/MVN@C NWs. (f) XRD patterns of MVN@C NWs and S/MVN@C NWs.

of few isolated mesopores with the size of 2–4 nm (Fig. S4b, Supporting information). The elemental mapping (Fig. 2c) and electron energy loss spectroscopy (EELS) line scans (Fig. S6) of S/MVN@C NWs boast the homogeneous distribution of S in the MVN@C NWs. The flexible and self-supporting S/MVN@C NWs cathode film is constructed by intertwining and interpenetrating S/MVN@C NWs without a mechanical supporter and conductive additive. The optical images indicate that the paper-like S/MVN@C NWs film with a thickness of about 15 μm exhibits excellent flexibility and mechanical integrity albeit under repetitive bending (Fig. 2d). The thermogravimetry (TG) analysis (Fig. 2e) indicates the S mass loading could reach as high as 82.6 wt%, corresponding to an area loading of 9.7 mg cm^{-2}. Since the S/MVN@C NWs with sulfur content of 57.2 wt% show the best electrochemical performance. Therefore, we use the sample with 57.2 wt% for further investigation. The XRD patterns in Fig. 2f can be indexed to orthorhombic elemental S (JCPDS No. 74-1465) except the diffraction peaks from cubic VN (JCPDS No. 73-0528). The S/MVN@C NWs offer a conductive 3D framework and strong chemical anchoring and physical trapping of polysulfide, thereby resulting in fast ion transport, high capacity, and excellent reversibility in Li-S batteries.

The coin-like cell with freestanding S/MVN@C NWs film as cathode and Li foil as counter anode was used to evaluate the electrochemical properties of S/MVN@C NWs. The S/MVN@C NWs film cathode exhibits a large capacity and high reversibility (Figs. 3a and S7, Supporting information) even at areal mass loading of 9.7 mg cm^{-2}. With an areal mass loading of 2.8 mg cm^{-2}, the materials deliver the largest reversible capacity of 1040 mAh g^{-1} at 1 C rate and this sample is chosen in subsequent studies. The Cyclic voltammogram (CV) profiles of the S/MVN@C NWs cathode at a sweeping rate of 0.1 mV s^{-1} in the potential window between 1.6 and 3.0 V (versus Li^+/Li) are shown in Fig. S8a (Supporting information). The two reduction peaks at 1.96 and 2.28 V are attributed to the formation of high-order Li_2S_n and short-chain insoluble lithium sulfide (Li_2S_2 or Li_2S). The two anodic peaks at 2.44 and 2.50 V represent the reactions from lithium sulfide to long-chain lithium polysulfide and S [35,36]. During cycling, the oxidation and reduction peaks become sharper and then stable after 5 cycles, indicating high reversibility. The charging/discharging profiles of the S/MVN@C NWs at different rates are presented in Fig. S8b (Supporting information). For comparison, the N-doping carbon nanotubes (NCNT) are prepared by removing the VN of MVN@C NWs in hot KOH solution and the S impregnated NCNT cathode is obtained with a similar S mass loading as S/NCNT. Fig. S9 (Supporting information) demonstrate the discharging profiles of the S/MVN@C NWs and S/NCNT at rate of 0.2 C, indicating two-plateaus of a typical sulfur cathode. The Q_1 and Q_2 are

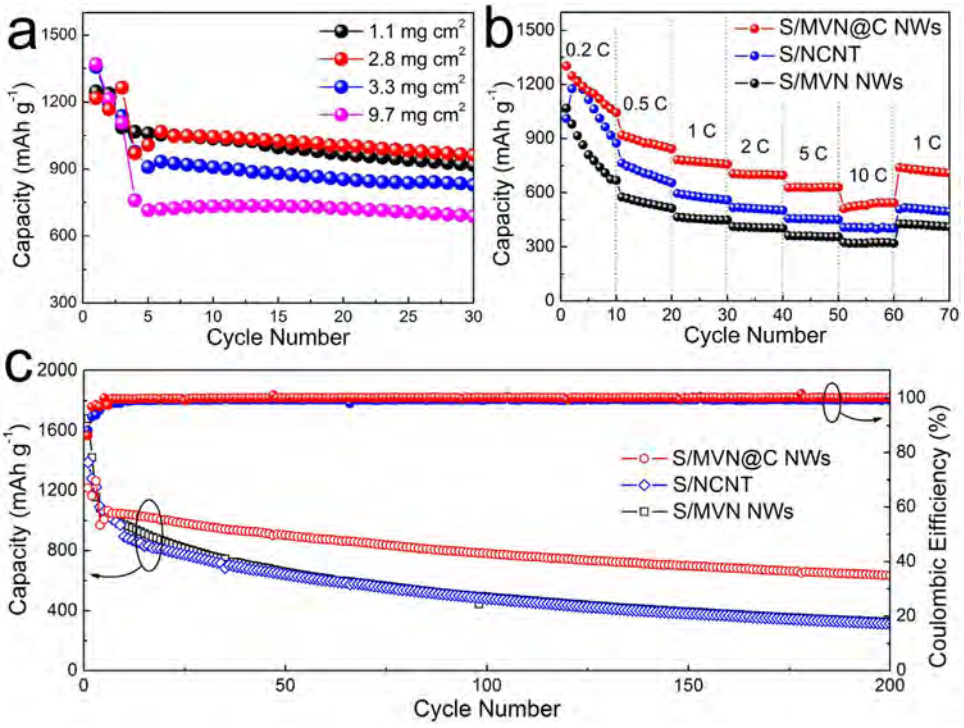

Fig. 3. (a) Cycling performance of S/MVN@C NWs with different areal S loading. (b) Rate performances of the electrodes at various current densities. (c) Cycling performance of S/MVN@C NWs, S/MVN NWs and S/NCNT at 1 C and corresponding Coulombic efficiency.

Table 1
Comparison of battery properties of S/MVN@C NWs and other S-based cathodes. (1 C = 1650 mA g^{-1}).

Materials	S content	Areal S mass loading	Cycling Stability	Rate Capability	Ref.
S/G-NDHCS	62.0 wt%	3.9 mg cm^{-2}	520 mAh g^{-1} after 200 cycles at 0.5 C	430 mAh g^{-1} at 3 C	[37]
S/PVPS/PED@RGO	52.2 wt%	0.62–0.85 mg cm^{-2}	420 mAh g^{-1} after 500 cycles at 1 C	428 mAh g^{-1} at 2 C	[38]
S/NG/CNT	53.0 wt%	4.7 mg cm^{-2}	882 mAh g^{-1} after 180cycles at 0.5 C	550 mAh g^{-1} at 2 C	[39]
S/G nanowalls	66.0 wt%		1220 mAh g^{-1} after 120 cycles at C/8	410 mAh g^{-1} at 8 C	[36]
S/C@WS_2	11 wt%	1.0–1.2 mg cm^{-2}	563 mAh g^{-1} after 1500 cycles at 2 C	448 mAh g^{-1} at 3 C	[20]
S/NiS_2	50 wt%	1.0 mg cm^{-2}	954 mAh g^{-1} after 1200 cycles at 0.3 C	730 mAh g^{-1} at 1.2 C	[40]
S/TiN	58.8 wt%	1.0 mg cm^{-2}	660 mAh g^{-1} after 200 cycles at 0.5 C	555 mAh g^{-1} at 5 C	[45]
S/WN		9.5 mg cm^{-2}	980 mAh g^{-1} after 100 cycles at 0.1 C	665 mAh g^{-1} at 1 C	[41]
S/MnO_2@HCF	58.8 wt%	3.5 mg cm^{-2}	662 mAh g^{-1} after 300 cycles at 0.5 C	690 mAh g^{-1} at 1 C	[23]
S/TiO2@HCNF	67.5 wt%	1.6 mg cm^{-2}	670 mAh g^{-1} after 200 cycles at 0.5 C	630 mAh g^{-1} at 1 C	[42]
S/Co_3O_4	42 wt%	0.8 mg cm^{-2}	656 mAh g^{-1} after 200 cycles at 0.2 C	350 mAh g^{-1} at 5 C	[43]
S/MgO	54 wt%	1.9 mg cm^{-2}	720 mAh g^{-1} after 100 cycles at 0.2 C	540 mAh g^{-1} at 2 C	[44]
S/MVN@C	57.2 wt%	2.8 mg cm^{-2}	636 mAh g^{-1} after 200 cycles at 1 C	782 mAh g^{-1} at 1 C 543 mAh g^{-1} at 10 C	This work

the discharge capacities in different stages, corresponding to the reduction of sulfur to high-order Li_2S_n ($S_8 \rightarrow S_6^{2-} \rightarrow S_4^{2-}$) and short-chain insoluble lithium sulfide (Li_2S_2 or Li_2S) ($S_4^{2-} \rightarrow Li_2S_2 \rightarrow Li_2S$). The capacity ratio of Q_2 to Q_1 (Q_2/Q_1) can reflect the catalytic ability for polysulfides reduction reaction [46,47]. The Q_2/Q_1 of S/MVN@C NWs is 2.51, higher than that of S/NCNT (1.98), which can be attributed to catalytic properties of VN for polysulfides reduction reaction. Since the VN could accelerate the charge transfer and promote conversion of polysulfides to Li_2S, the plateau of Q_2 for S/MVN@C NWs exhibit larger capacity compared to S/NCNT. [29,48]. The discharging and charging voltage plateaus of the S/MVN@C NWs cathode at a large current density of 10 C can be clearly observed, further suggesting low polarization and fast redox reaction dynamics. Fig. 3b discloses the rate capability of S/MVN@C NWs, S/MVN NWs and S/NCNT. The S/MVN@C NWs cathode is superior to the S/MVN NWs and S/NCNT cathodes in terms of capacities at all current densities. At a large current density of 10 C, the S/MVN@C NWs cathode still delivers a capacity of 543 mAh g^{-1}, which is much higher than those of the previously-reported S-based cathodes (Table 1) [20,23,36–45]. When the current is restored to 1 C after 60 cycles, the discharge capacity of the S/MVN@C NWs cathode remains at 740 mAh g^{-1} indicating perfect stability and high reversibility. The long-term cycle performance of the S/MVN@C NWs, S/NCNT and S/MVN NWs cathodes is shown in Fig. 3c. The first 3 cycles are measured at 0.2 C rate for gradual activation and the following at 1 C rate. The S/MVN@C NWs cathode delivers a reversible capacity of 1040 mAh g^{-1} after 10 cycles, which is much larger than those of S/MVN NWs and S/NCNT cathodes. Moreover, the capacity of the S/MVN@C NWs cathodes remains a high capacity of 636 mAh g^{-1} after 200 cycles. Although the NCNT and MVN NWs have been reported to improve the performance of Li-S batteries [29,49], the electrochemical performance of the S/MVN@C NWs cathode is much better than that of S/NCNT and S/MVN NWs cathodes under the same conditions. Our results demonstrate that the S/MVN@C NWs films still exhibit a high conductivity of 2.3 × 10^4 Ω^{-1} m^{-1} after S impregnation with 57.2% content. Therefore, the large capacity and good rate capability of the S/MVN@C NWs cathodes can be attributed to the high conductivity of network of S/MVN@C NWs and dual physical and chemical confinement effects for polysulfides.

To verify the physical trapping and strong chemical anchoring of MVN@C NWs for polysulfides, the adsorption capabilities of MVN@C NWs, MVN NWs, and NCNT towards polysulfides are compared (Fig. 4a). Equivalent amounts (25 mg) of MVN@C NWs, MVN NWs, and

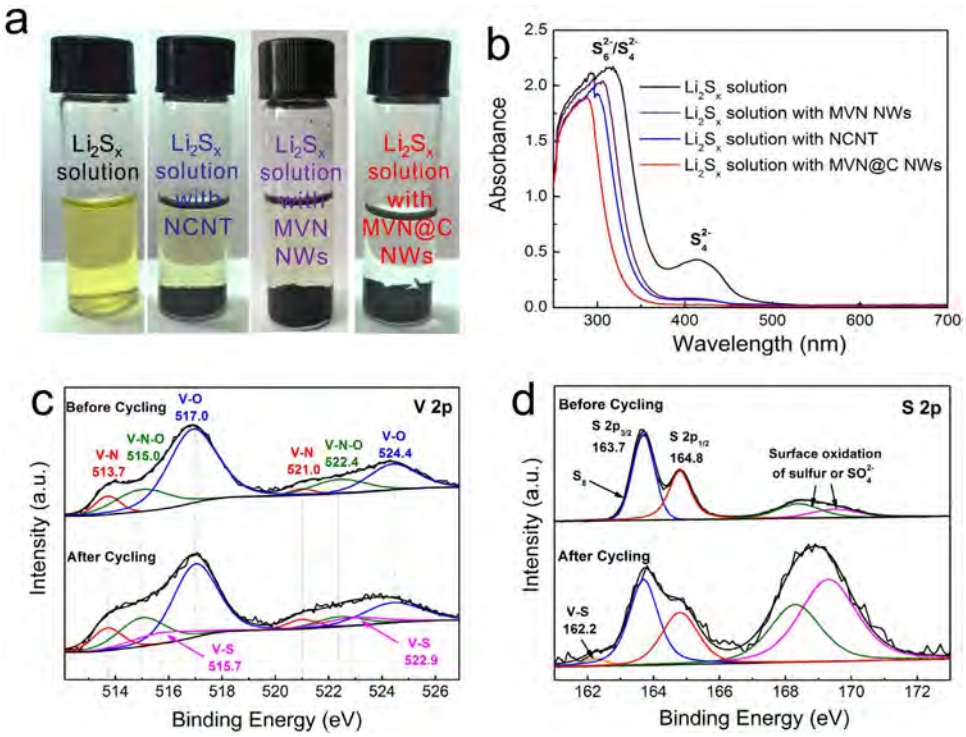

Fig. 4. (a) Digital pictures of adsorption performance of MVN@C NWs, MVN NWs and NCNT towards polysulfides. (b) UV–Vis absorption spectra of the Li_2S_6 solution after adding MVN@C NWs, MVN NWs and NCNT. (c) High-resolution V 2p and (d) S 2p XPS spectra of S/MVN@C NWs before and after 200 cycles.

NCNT are added to 3 mL of the orange Li_2S_6 solution (5 mM). After 24 h, the color of polysulfide solution containing MVN@C NWs turns colorless, whereas the solution containing the MVN NWs and NCNT shows white yellow and bright yellow, respectively. The ultraviolet-visible (UV–Vis) spectra are used to quantitatively determine the concentration change in the Li_2S_6 solution after adding NCNT, MVN NWs, or MVN@C NWs, as shown in Fig. 4b. The sharp peaks at 315 and 410 nm are attributed to S_6^{2-}/S_4^{2-} and S_4^{2-}, respectively [45,50]. The absorption peak of Li_2S_6 at 410 nm disappears after adding MVN@C NWs, while the absorption peaks of S_6^{2-}/S_4^{2-} and S_4^{2-} species become weaker after adding MVN NWs compared to the sample added with NCNT. The strong chemical adsorption ability of MVN@C NWs towards polysulfides is due to the formation of polar bonding of V-S as evidenced by X-ray photoelectron spectroscopy (XPS) in Figs. 4c-d acquired from S/MVN@C NWs before and after 200 cycles. The XPS survey spectra reveal the presence of small amounts of V-N-O and V-O bonds in addition to V-N [51–54], which offer high affinity to polar polysulfide resulting in strong chemical absorption. After 200 cycles, the survey spectra of V and S reveal the formation of S-V bonding at 515.7 eV (V 2p) and 162.2 eV (S 2p) [55–57], suggesting chemical binding between VN and polysulfide. The SEM images of the S/MVN@C NWs electrode before and after 200 cycles at 1 C are depicted in Fig. 5. The morphology of S/MVN@C NWs remains intact and no obvious polysulfide intermediates are observed from the cathode further proving the high structural stability of S/MVN@C NWs. The HR-TEM and corresponding elemental mapping images of S/MVN@C NWs after 200 cycles at 1 C (as shown in Figs. S10 and 11) demonstrating the nanowire structure remain intact and S, V and C are uniformly in S/MVN@C NWs, further proving the high structural stability of S/MVN@C NWs. The high structural stability of S/MVN@C NW is attributed to the core-shell morphology, stable mesoporous VN and the enough empty space in the inner MVN to buffer the stress originating from the S volume changes during charging/discharging processes.

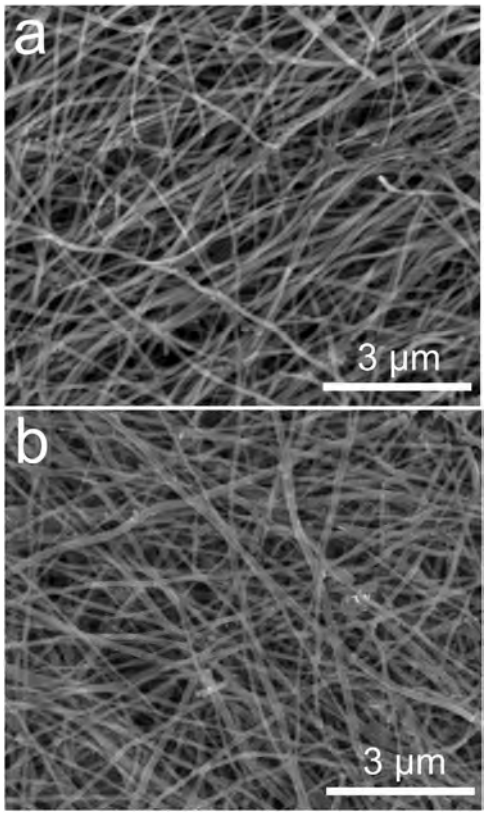

Fig. 5. SEM images of S/MVN@C NWs before (a) and after (b) 200 cycles at a 1 C rate.

4. Conclusions

In summary, we have demonstrated the synthesis of the S nanodots embedded into the core-shell MVN@C NWs by a melt-diffusion process. This freestanding flexible film electrode comprising of 3D intertwined S impregnated MVN@C NWs shows a high reversible capacity of 636 mAh g^{-1} after 200 cycles at a current density of 1 C and high rate performance with a capacity of 543 mAh g^{-1} at 10 C. Our results demonstrate that microporous C coating and conductive mesoporous VN provide strong physical trapping and chemical anchoring towards S and

polysulfides and thus 3D conductive network of S/MVN@C NWs facilitate electron and ion transportation. Therefore, the freestanding film electrode of S/MVN@C NWs exhibits high rate capability, large capacity and long cycle stability. Our results indicate that the introduction of a mesoporous and conductive polar VN into microporous C shell is a feasible strategy for S host to achieve large capacity, high rate performance and stability, which offers potential applications for high-energy Li-S batteries.

Acknowledgments

This work was financially supported by National Natural Science Foundation of China (Nos. 51572100, 51504171 and 61434001), Outstanding Young and Middle-aged Scientific Innovation Team of Colleges and Universities of Hubei Province (T201402), Natural Science Foundation of Hubei Province (2015CFA116), Project of Hubei Provincial Education Office (B2015346), HUST Key Interdisciplinary Team Project (2016JCTD101) and City University of Hong Kong Applied Research Grant (No. 9667104). The authors also acknowledge the Analytical and Testing Center of HUST for providing characterization facilities.

Appendix A. Supplementary material

Supplementary data associated with this article can be found in the online version at http://dx.doi.org/10.1016/j.nanoen.2017.09.018.

References

[1] M.S. Whittingham, Chem. Rev. 114 (2014) 11414–11443.
[2] N. Alias, A.A. Mohamad, J. Power Sources 274 (2015) 237–251.
[3] J.L. Wang, Y.S. He, J. Yang, Adv. Mater. 27 (2015) 569–575.
[4] A. Rosenman, E. Markevich, G. Salitra, D. Aurbach, A. Garsuch, F.F. Chesneau, Adv. Energy Mater. 5 (2015) 1500212.
[5] R.P. Fang, S.Y. Zhao, Z.H. Sun, D.W. Wang, H.M. Cheng, F. Li, Adv. Mater. 29 (2017) 1606823.
[6] L. Sun, D.T. Wang, Y.F. Luo, K. Wang, W.B. Kong, Y. Wu, L.N. Zhang, K.L. Jiang, Q.Q. Li, Y.H. Zhang, J.P. Wang, S.S. Fan, ACS Nano 10 (2016) 1300–1308.
[7] H.W. Chen, C.H. Wang, W.L. Dong, W. Lu, Z.L. Du, L.W. Chen, Nano Lett. 15 (2015) 798–802.
[8] S.T. Zhang, M.B. Zheng, Z.X. Lin, N.W. Li, Y.J. Liu, B. Zhao, H. Pang, J.M. Cao, P. He, Y. Shi, J. Mater. Chem. A 2 (2014) 15889–15896.
[9] W.D. Zhou, X.C. Xiao, M. Cai, L. Yang, Nano Lett. 14 (2014) 5250–5256.
[10] W.M. Kang, N.P. Deng, J.G. Ju, Q.X. Li, D.Y. Wu, X.M. Ma, L. Li, M. Naebe, B.W. Cheng, Nanoscale 8 (2016) 16541–16588.
[11] Z.W. Seh, Y.M. Sun, Q.F. Zhang, Y. Cui, Chem. Soc. Rev. 45 (2016) 5605–5634.
[12] S.K. Lee, S.M. Oh, E. Park, B. Scrosati, J. Hassoun, M.S. Park, Y.J. Kim, H. Kim, I. Belharouak, Y.K. Sun, Nano Lett. 15 (2015) 2863–2868.
[13] M.P. Yu, J.S. Ma, H.Q. Song, A.J. Wang, F.Y. Tian, Y.S. Wang, H. Qiu, R.M. Wang, Energy Environ. Sci. 9 (2016) 1495–1503.
[14] M.P. Yu, W.J. Yuan, C. Li, J.D. Hong, G.Q. Shi, J. Mater. Chem. A 2 (2014) 7360–7366.
[15] H. Kim, J.T. Lee, D.C. Lee, A. Magasinski, W. Cho, G. Yushin, Adv. Energy Mater. 3 (2013) 1308–1315.
[16] X. Liang, C. Hart, Q. Pang, A. Garsuch, T. Weiss, L.F. Nazar, Nat. Commun. 6 (2015) 5682–5690.
[17] Q. Pang, D.P. Kundu, M. Cuisinier, L.F. Nazar, Nat. Commun. 5 (2014) 4759–4767.
[18] X. Liang, C.Y. Kwok, F.L. Marzano, Q. Pang, M. Cuisinier, H. Huang, C.J. Hart, D. Houtarde, K. Kaup, H. Sommer, T. Brezesinski, J. Janek, L.F. Nazar, Adv. Energy Mater. 6 (2016) 1501636.
[19] Z.W. Seh, J.H. Yu, W.Y. Li, P.C. Hsu, H.T. Wang, Y.M. Sun, H.B. Yao, Q.F. Zhang, Y. Cui, Nat. Commun. 5 (2014) 5017–5024.
[20] T.Y. Lei, W. Chen, J.W. Huang, C.Y. Yan, H.X. Sun, C. Wang, W.L. Zhang, Y.R. Li, J. Xiong, Adv. Energy Mater. 7 (2017) 1601843.
[21] Z. Yuan, H.J. Peng, T.Z. Hou, J.Q. Huang, C.M. Chen, D.W. Wang, X.B. Cheng, F. Wei, Q. Zhang, Nano Lett. 16 (2016) 519–527.
[22] X. Liang, A. Garsuch, L.F. Nazar, Angew. Chem. Int. Ed. 54 (2015) 3907–3911.
[23] Z. Li, J.T. Zhang, X.W. Lou, Angew. Chem. Int. Ed. 54 (2015) 12886–12890.
[24] Q. Pang, X. Liang, C.Y. Kwok, L.F. Nazar, J. Electrochem. Soc. 162 (2015) A2567–A2576.
[25] X. Xiao, X. Peng, H.Y. Jin, T.Q. Li, C.C. Zhang, B. Gao, B. Hu, K.F. Huo, J. Zhou, Adv. Mater. 25 (2013) 5091–5097.
[26] P.H. Yang, D.L. Chao, C.R. Zhu, X.H. Xia, Y.Q. Zhang, X.L. Wang, P. Sun, B.K. Tay, Z.X. Shen, W.J. Mai, H.J. Fan, Adv. Sci. 3 (2016) 1500299.
[27] G.Q. Ma, Z. Wang, B. Gao, T.P. Ding, Q.Z. Zhong, X. Peng, J. Su, B. Hu, L.Y. Yuan, P.K. Chu, J. Zhou, K.F. Huo, J. Mater. Chem. A 3 (2015) 14617–14624.
[28] Z.M. Cui, C.X. Zu, W.D. Zhou, A. Manthiram, J.B. Goodenough, Adv. Mater. 28 (2016) 6926–6931.
[29] Z.H. Sun, J.Q. Zhang, L.C. Yin, G.J. Hu, R.P. Fang, H.M. Cheng, F. Li, Nat. Commun. 8 (2017) 14627–14634.
[30] Y. Zhang, J.Y. Lai, Y.D. Gong, Y.M. Hu, J. Liu, C.W. Sun, Z.L. Wang, ACS Appl. Mater. Interfaces 8 (2016) 34309–34316.
[31] X.X. Li, W.Y. Li, H. Ma, J. Chen, J. Electrochem. Soc. 154 (2007) A39–A42.
[32] Z. Chen, V. Augustyn, J. Wen, Y.W. Zhang, M.Q. Shen, B. Dunn, Y.F. Lu, Adv. Mater. 23 (2011) 791–795.
[33] B. Gao, X.X. Li, X.L. Guo, X.M. Zhang, X. Peng, L. Wang, J.J. Fu, P.K. Chu, K.F. Huo, Adv. Mater. Interfaces 2 (2015) 1500211.
[34] K.L. Ai, Y.L. Liu, C.P. Ruan, L.H. Lu, G.Q. Lu, Adv. Mater. 25 (2013) 998–1003.
[35] X. Yang, L. Zhang, F. Zhang, Y. Huang, Y.S. Chen, ACS Nano 8 (2014) 5208–5215.
[36] B. Li, S.M. Li, J.H. Liu, B. Wang, S.B. Yang, Nano Lett. 15 (2015) 3073–3079.
[37] G.M. Zhou, Y.B. Zhao, A. Manthiram, Adv. Energy Mater. 5 (2015) 1402263.
[38] Z.Y. Wang, J.L. Cheng, W. Ni, L.Z. Gao, D. Yang, J.M. Razal, B. Wang, J. Power Sources 342 (2017) 772–778.
[39] P.Y. Zhai, J.Q. Huang, L. Zhu, J.L. Shi, W.C. Zhu, Q. Zhang, Carbon 111 (2017) 493–501.
[40] Z. Liu, X. Zheng, S.L. Luo, S.Q. Xu, N.Y. Yuan, J.N. Ding, J. Mater. Chem. A 4 (2016) 13395–13399.
[41] N. Mosavati, S.O. Salley, K.Y. Simon Ng, J. Power Sources 340 (2017) 210–216.
[42] Z.A. Zhang, Q. Li, S.F. Jiang, K. Zhang, Y.Q. Lai, J. Li, Chem. Eur. J. 21 (2015) 1343–1349.
[43] H.Q. Wang, T.F. Zhou, D. Li, H. Gao, G.P. Gao, A.J. Du, H.K. Liu, Z.P. Guo, ACS Appl. Mater. Interfaces 9 (2017) 4320–4325.
[44] R. Ponraj, A.G. Kannan, J.H. Ahn, D.W. Kim, ACS Appl. Mater. Interfaces 8 (2016) 4000–4006.
[45] Z.X. Hao, L.X. Yuan, C.J. Chen, J.W. Xiang, Y.Y. Li, Z.M. Huang, P. Hu, Y.H. Huang, J. Mater. Chem. A 4 (2016) 17711–17717.
[46] J.W. Zhou, R. Li, X.X. Fan, Y.F. Chen, R.D. Han, W. Li, J. Zheng, B. Wang, X.G. Li, Energy Environ. Sci. 7 (2014) 2715–2724.
[47] D.W. Su, M. Cortie, H.B. Fan, G.X. Wang, Adv. Mater. (2017), http://dx.doi.org/10.1002/adma.201700587.
[48] H.A. Salem, G. Babu, C.V. Rao, L.M.R. Arava, J. Am. Chem. Soc. 137 (2015) 11542–11545.
[49] Q. Li, Z.A. Zhang, Z.P. Guo, Y.Q. Lai, K. Zhang, J. Li, Carbon 78 (2014) 1–9.
[50] Z.B. Xiao, Z. Yang, L. Wang, H.G. Nie, M.E. Zhong, Q.Q. Lai, X.J. Xu, L.J. Zhang, S.M. Huang, Adv. Mater. 27 (2015) 2891–2898.
[51] E.F. de Souza, C.A. Chagas, T.C. Ramalho, V.T. da Silva, D.L.M. Aguiar, R.S. Gil, R.B. de Alencastro, J. Phys. Chem. C 117 (2013) 25659–25668.
[52] J. Mendialdua, R. Casanova, Y. Barbaux, J. Electron. Spectrosc. Relat. Phenom. 71 (1995) 249–261.
[53] C.M. Ghimbeu, E. Raymundo-Piñero, P. Fioux, F. Béguin, C. Vix-Gute, J. Mater. Chem. 21 (2011) 13268–13275.
[54] X.H. Lu, M.H. Yu, T. Zhai, G.M. Wang, S.L. Xie, T.Y. Liu, C.L. Liang, Y.X. Tong, Y. Li, Nano Lett. 13 (2013) 2628–2633.
[55] D.Q. Gao, Q.X. Xue, X.Z. Mao, W.X. Wang, Q. Xu, D.S. Xue, J. Mater. Chem. C. 1 (2013) 5909–5916.
[56] T.M. Masikhwa, F. Barzegar, J.K. Dangbegnon, A. Bello, M.J. Madito, D. Momodu, N. Manyala, RSC Adv. 6 (2016) 38990–39000.
[57] C.S. Rout, R. Khare, R.V. Kashid, D.S. Joag, M.A. More, N.A. Lanzillo, M. Washington, S.K. Nayak, D.J. Late, J. Inorg. Chem. 31 (2014) 5331–5336.

Xingxing Li received his B.E. degree in Material Science from Wuhan University of Science and Technology in 2013. Now he is a Ph.D. candidate under the supervision of Prof. Kaifu Huo in the State Key Laboratory of Refractories and Metallurgy at Wuhan University of Science and Technology. His research interests focus on synthesis of functional nanomaterials for energy storage.

Kang Ding received his B.E. degree in Material Science from Wuhan University of Science and Technology in 2015, and is currently a M.S. candidate under the supervision of Prof. Jijiang Fu in the State Key Laboratory of Refractories and Metallurgy at Wuhan University of Science and Technology. His main research interests are carbon nanostructures in the applications of lithium sulfur batteries and sodium ion batteries.

Biao Gao received his M.S. and Ph.D. in Material Science from Wuhan University of Science and Technology in 2012 and 2016. He is currently a lecture in the State Key Laboratory of Refractories and Metallurgy at Wuhan University of Science and Technology. His main research activity includes nanostructures for electrochemical energy storage.

Qingwei Li received his B.E. degree (2007) from Chang'an University and received M.S. degree (2011) from Henan University. Now, he is a Ph.D. candidate in the Wuhan National Laboratory for Optoelectronics (WNLO) at Huazhong University of Science and Technology (HUST), under the supervision of Prof. Kaifu Huo. His research interests focus on the controllable synthesis of nanomaterials for energy storage and conversion.

Yuanyuan Li received her M.S. degree from Key Laboratory for Special Functional Materials of the Ministry of Education, Henan University, China in 2013 and Ph.D. degree in the Wuhan National Laboratory for Optoelectronics (WNLO), Huazhong University of Science and Technology (HUST) in 2017. Currently, he is an assistant professor in Zhongyuan University of Technology. Her present research interests mainly focus on Li-S batteries

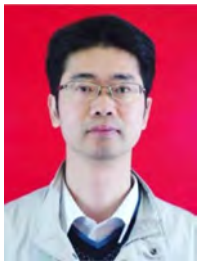

Jijiang Fu received his B.S. in Chemistry from Nanchang University in 1993 and Ph.D. in Physical Chemistry from Nanjing University (China) in 2005. He is currently a professor of materials science at Wuhan University of Science and Technology. His current research focuses on bioactive nanomaterials and nanostructured electrode materials for electrochemical biosensors and energy storage devices

Xuming Zhang received his Ph.D. in materials science and engineering from City University of Hong Kong in 2015 and worked for one year as a senior research associate in the Plasma Laboratory at City University of Hong Kong. He is now working as professor in Wuhan University of Science and Technology. His research interests on the synthesis of nanomaterials for application in electrochemical sensors and electrochemical energy storage devices

Paul K. Chu received his Ph.D. in Chemistry from Cornell University. He is Chair Professor of Materials Engineering in the Department of Physics and Materials Science at City University of Hong Kong. He is Fellow of the American Physical Society (APS), American Vacuum Society (AVS), Institute of Electrical and Electronics Engineers (IEEE), Materials Research Society (MRS), and Hong Kong Institution of Engineers (HKIE). He is also Fellow of the Hong Kong Academy of Engineering Sciences (HKAES). His research interests are quite diverse encompassing plasma surface engineering, materials science and engineering, surface science, and functional materials

Kaifu Huo received his B.S. in Applied Chemistry from China University of Petroleum in 1997 and a Ph.D. in Physical Chemistry from Nanjing University (China) in 2004. He is currently a Professor in the National Laboratory for Optoelectronics at Huazhong University of Science and Technology. He is an associate editor of Nanoscience and Nanotechnology Letters (NNL). He has authored/co-authored more than 100 papers in international refereed journals, which are cited more than 4000 times. His main research activities encompass bioactive nanomaterials and nanostructured electrode materials for electrochemical biosensors and energy storage devices.

Supporting Information

Freestanding Carbon Encapsulated Mesoporous Vanadium Nitride Nanowires Enable Highly Stable Sulfur Cathodes for Lithium-Sulfur Batteries by Chemical Anchoring and Physical Trapping of Polysulfides

Xingxing Li [a], Kang Ding [a], Biao Gao [a,*], Qingwei Li [b], Yuanyuan Li [b], Jijiang Fu [a], Xuming Zhang [a], Paul K Chu [c], Kaifu Huo [b,*]

[a] The State Key Laboratory of Refractories and Metallurgy, School of Materials and Metallurgy, Wuhan University of Science and Technology, Wuhan 430081 , China.

[b] Wuhan National Laboratory for Optoelectronics (WNLO) and School of Optical and Electronic Information, Huazhong University of Science and Technology, Wuhan 430074 , China.

[c] Department of Materials Science and Physics, City University of Hong Kong, Tat Chee Avenue, Kowloon, Hong Kong, China.

* Corresponding author:

E-mail: gaobiao@wust.edu.cn (Biao Gao); kfhuo@hust.edu.cn (Kaifu Huo)

The conductivity measurement of the film electrodes

The schematic of electrical conductivity measurements on a thin film via four-probe method is shown in Fig. S.[1] Firstly, four (i.e., point-like) probes with equal spacing (S) are placed linearly onto the surface of the film sample, and press at a certain pressure to make point contacts. The certain current (I) is passed through the two outer electrodes (1 and 4), a voltage (V) is obtained between the two center points 2 and 3. When the thickness of the electrode film (d, about 15 μm) is much smaller than the probe spacing (S, 1mm), the conductivity (σ) of electrode film can be calculated by the equation 1,[1-4] as below showing:

$$\sigma = \left(\frac{\ln 2}{\pi}\right)\frac{I}{dV} \qquad (1)$$

The $\frac{\ln 2}{\pi}$ is related to the ratio of S and d, where S is the spacing distance of probes and d is the film thickness.

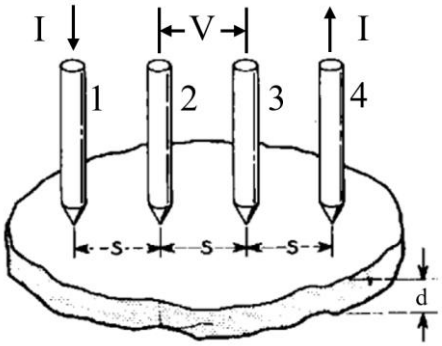

Fig. S. Graphical illustrations of electrical conductivity measurements on a thin film.[1]

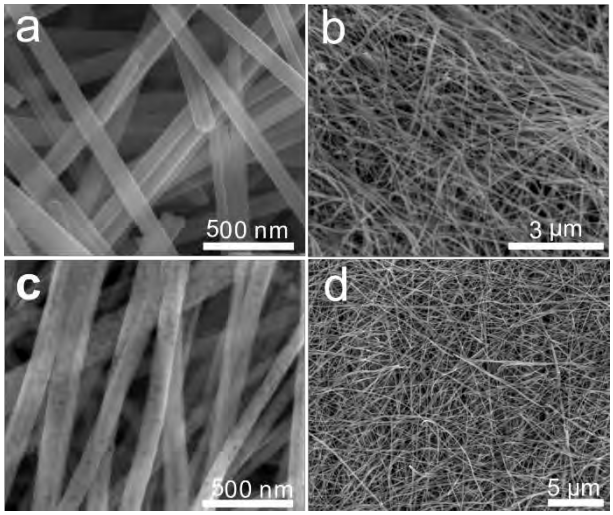

Fig. S1. SEM images: (a, b) V_2O_5 NWs and (c, d) MVN@C NWs.

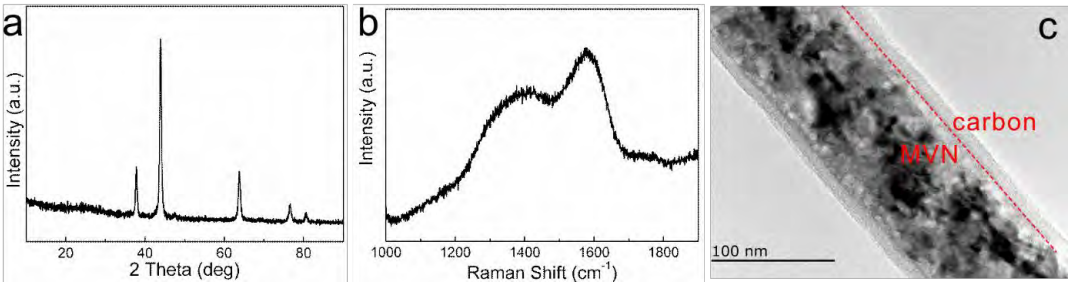

Fig. S2. (a) XRD spectrum, (b) Raman scattering spectrum, and (c) TEM image of MVN@C NWs.

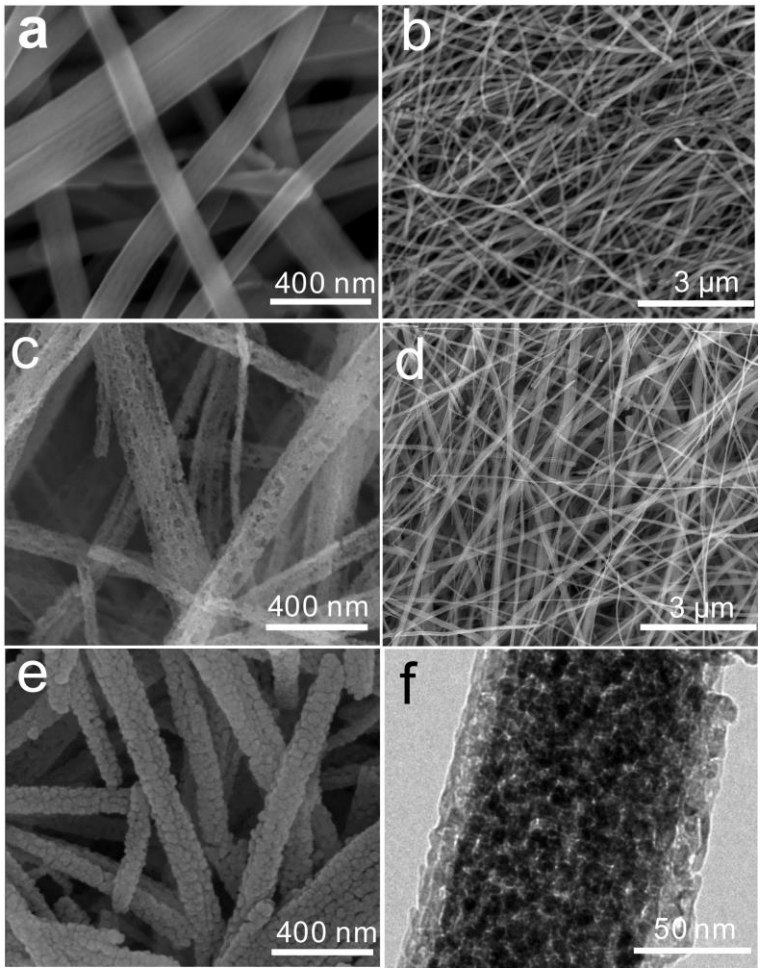

Fig. S3. SEM images of S/MVN@C NWs (a, b), MVN NWs (c, d) and S/MVN NWs (e). TEM image of S/MVN NWs (f).

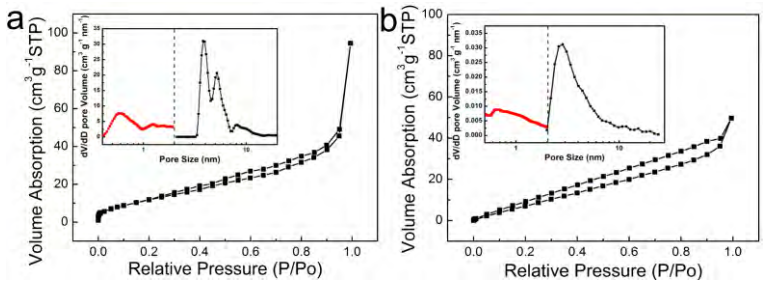

Fig. S4. Nitrogen gas adsorption-desorption isotherms of (a) MVN@C NWs and (b) S/MVN@C NWs with the insets indicating pore size distribution.

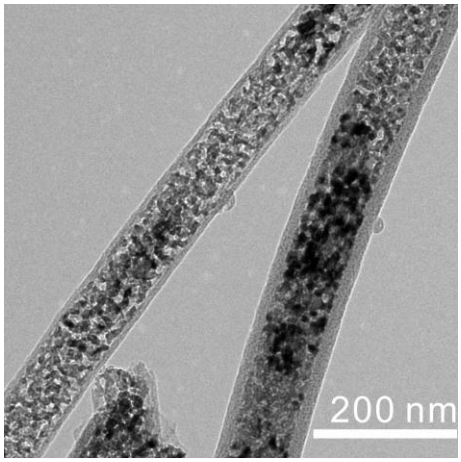

Fig. S5. TEM image of S/MVN@C NWs after full lithiation.

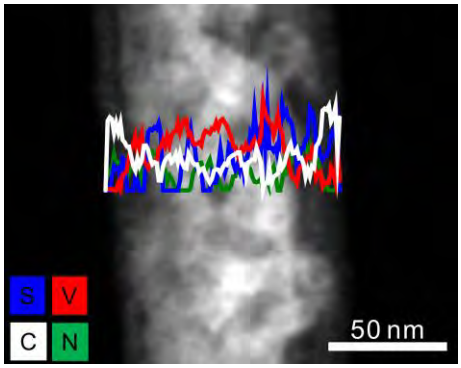

Fig. S6. HRTEM and corresponding EELS line scans of S/MVN@C NWs.

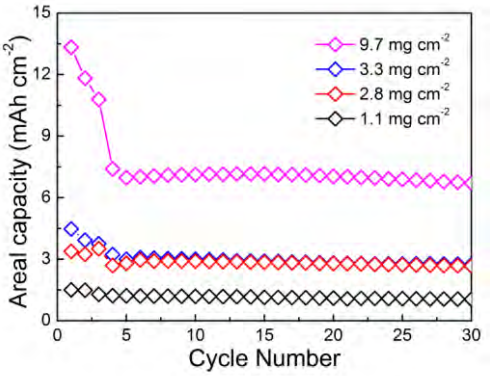

Fig. S7. Areal capacitance of S/MVN@C NWs with different sulfur mass loading.

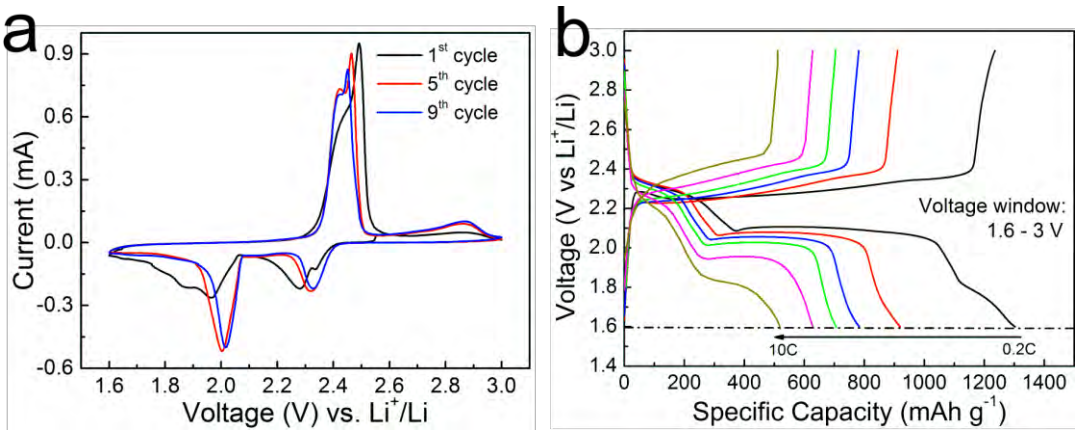

Fig. S8. (a) CV curves and (b) Charging-discharging voltage profiles of S/MVN@C NWs at current densities from 0.2 to 10 C.

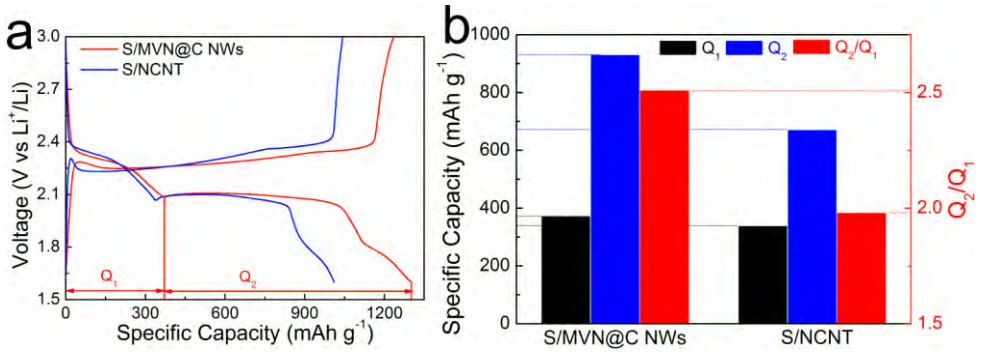

Fig. S9. (a) A typical voltage profile of the S/MVN@C NWs and S/NCNT at 0.2 C, (b) Q_1 and Q_2 are the discharge capacities in stages 1 ($S_8 + 4e^- + 4Li^+ \leftrightarrow 2Li_2S_4$) and 2 ($Li_2S_4 + 6e^- + 6Li^+ \leftrightarrow 4Li_2S$), respectively.

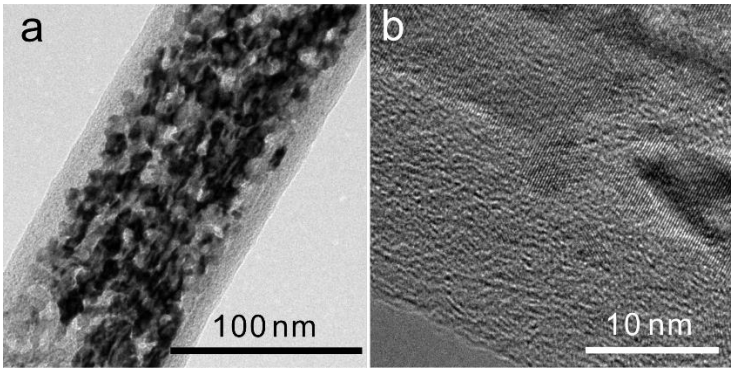

Fig. S10. TEM and HRTEM image S/MVN@C NWs after 200 cycles.

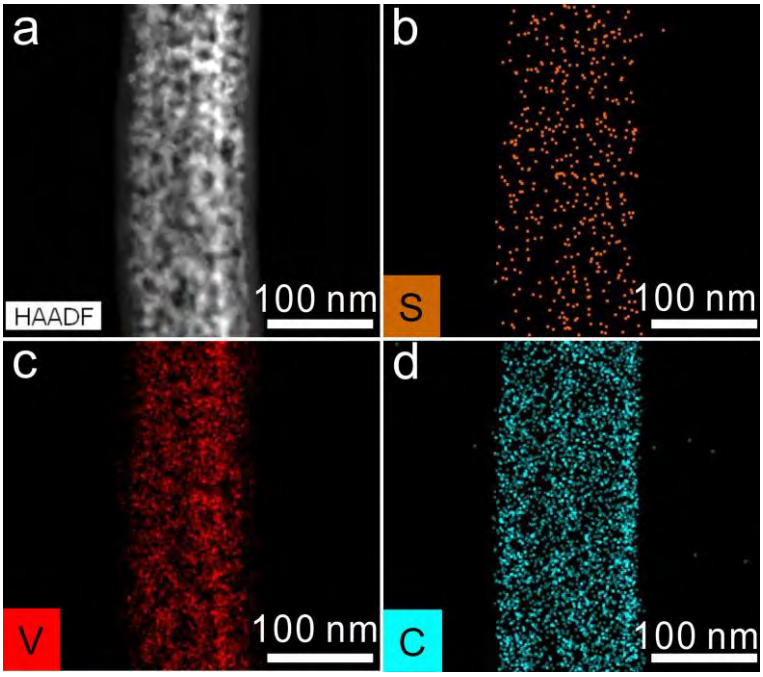

Fig. S11. (a) STEM image of S/MVN@C NWs after cycling with the corresponding elemental maps of (b) sulfur, (c) vanadium and (d) carbon.

Reference

[1] F. Smits, Bell Syst. Tech. J. 37 (1958) 711-718.

[2] L. B. Valdes, Proc. IRE 42 (1954) 420-42.

[3] L. Sun, M. G. Campbell, M. Dinca, Angew. Chem. Int. Ed. 55 (2016) 3566-3579.

[4] Lei Sun, Sarah S. Park, Dennis Sheberla, and Mircea Dinca, J. Am. Chem. Soc. 138 (2016) 14772-14782.

.